Aerosol Science and Technology

ISSN: 0278-6826 (Print) 1521-7388 (Online) Journal homepage: www.tandfonline.com/journals/uast20

Accurate Determination of Aerosol Activity Coefficients at Relative Humidities up to 99% Using the Hygroscopicity Tandem Differential Mobility Analyzer Technique

Sarah R. Suda & Markus D. Petters

To cite this article: Sarah R. Suda & Markus D. Petters (2013) Accurate Determination of Aerosol Activity Coefficients at Relative Humidities up to 99% Using the Hygroscopicity Tandem Differential Mobility Analyzer Technique, Aerosol Science and Technology, 47:9, 991-1000, DOI: 10.1080/02786826.2013.807906

To link to this article: https://doi.org/10.1080/02786826.2013.807906

Published online: 18 Jun 2013.

Aerosol Science and Technology, 47:991–1000, 2013

ISSN: 0278-6826 print / 1521-7388 online
DOI: 10.1080/02786826.2013.807906

Accurate Determination of Aerosol Activity Coefficients at Relative Humidities up to 99% Using the Hygroscopicity Tandem Differential Mobility Analyzer Technique

Sarah R. Suda and Markus D. Petters

Department of Marine, Earth and Atmospheric Sciences, North Carolina State University, Raleigh, North Carolina, USA

Aerosol water content plays an important role in aqueous phase reactions, in controlling visibility, and in cloud formation processes. One way to quantify aerosol water content is to measure hygroscopic growth using the hygroscopicity tandem differential mobility analyzer (HTDMA) technique. However, the HTDMA technique becomes less reliable at relative humidity (RH) >90% due to the difficulty of controlling temperature and RH inside the second DMA. For this study, we have designed and implemented a new HTDMA system with improved temperature and RH control. Temperature stability in the second DMA was achieved to ±0.02°C tolerance by implementing active control using thermoelectric heat exchangers and PID control loops. The DMA size resolution was increased by operating high-flow DMA columns at a sheath:sample flow ratio of 15:0.5. This improved size resolution allowed for improving the accuracy of the RH sensors by interspersing ammonium sulfate reference scans at high frequency. We present growth factor data for pure compounds at RH up to 99% and compare the data to theoretical values and to available bulk water activity data. With this HTDMA instrument and method, the osmotic coefficients of spherical, nonvolatile aerosols of known composition between 30 and 200 nm in diameter can be determined within ±20%. We expect that data from this instrument will lead to an improvement of aerosol water content models by contributing to the understanding of aerosol water uptake at high RH.

1. INTRODUCTION

Ambient aerosols take up water in humid air and serve as condensation nuclei for haze and cloud droplets. Uncertainty in aerosol water uptake contributes to the uncertainty in estimates of aerosol water content and hinders studies that extrapolate measured hygroscopic growth factors to predict a particle's ability to serve as a cloud condensation nucleus (Prenni et al. 2007). Aerosol water content is determined by the ambient RH and the associated chemical composition dependent hygroscopicity of the aerosol. Particle hygroscopicity is a measure that scales the volume of water associated with a unit volume of dry particle (Petters and Kreidenweis 2007) and depends on the molar volume and the activity coefficients of the dissolved compounds (Christensen and Petters 2012). Activity coefficients cannot be obtained by modeling alone because nonideal interactions between compounds remain largely unexplained on the molecular level. One of the main difficulties is the lack of experimental data to constrain activity coefficient models (Topping et al. 2005; Amundson et al. 2007) for likely constituents of atmospheric aerosols (Raatikainen and Laaksonen 2005). Of particular interest are activity coefficients for compounds frequently identified in organic aerosols at RH approaching 100%. For example, Petters et al. (2009) show that for some secondary organic aerosol water uptake is highly nonideal at RH ∼90% and becomes more ideal when approaching RH 100%. Understanding this transition is important for linking aerosol water uptake and cloud condensation nuclei activity in a unified aerosol modeling framework.

The hygroscopicity tandem differential mobility analyzer (HTDMA) technique (Rader and McMurry 1986) is used to measure the diameter growth factor of aerosol particles at a controlled RH. Two differential mobility analyzers (DMAs) characterize the aerosol size before and after its passage through a humidification setup. The resulting humidified size is compared to the dry size and a single growth factor, gf, is computed to describe the aerosol's water uptake:

$$gf = \frac{D}{D_d}, \quad [1]$$

where D is the humidified droplet mobility diameter and D_d is the particle dry mobility diameter. Controlling RH accurately

Received 29 November 2012; accepted 28 April 2013.

This work was funded by the Office of Science (BER), U.S. Department of Energy, under DESC0006633. We thank Patrick Chuang and Sonia Kreidenweis for the high-flow DMA columns and Tim Wright for help with instrument construction.

Address correspondence to Markus D. Petters, Department of Marine, Earth and Atmospheric Sciences, North Carolina State University, Campus Box 8208, Raleigh, NC 27695-8208, USA. E-mail: markus_petters@ncsu.edu

inside the second DMA is challenging. Small variations in dew point temperature (T_{dew}) and temperature (T) result in large excursions in RH. For example, at RH = 99% the dew point depression ($T - T_{dew}$) is ~0.6 K, thereby necessitating highly accurate temperature and moisture control to keep random RH fluctuations within acceptable tolerance. One approach to address this problem is to submerge the second DMA in a temperature-controlled water bath to minimize temperature gradients inside the column (Weingartner et al. 2002; Hennig et al. 2005). The setup described by Hennig et al. (2005) allows growth factor measurements up to 98% RH, but the quoted precision in RH (±1.2% in absolute units at RH = 97.7%) and diameter growth factor (±0.46 in absolute units at $gf = 2.79$) results in ±121% relative uncertainty in the retrieved hygroscopicity parameter for 100 nm dry aerosol, where uncertainty is defined as the maximum difference between the hygroscopicity at the given RH and gf values and that at the edges of the ranges provided in their Table 2. Controlling and accurately measuring T_{dew} is also extremely challenging. The most accurate direct measurement for humidity is the chilled-mirror dew point hygrometer (Barrett and Herndon 1951), which can achieve accuracy of $T_{dew} \sim \pm 0.1$ K and precision of 0.01 K. Control of T_{dew} at or near water saturation is contingent on temperature control because patchy cold spots in the system can cause condensation.

The width of the DMA transfer function is dictated by the sheath:sample flow ratio (Knutson and Whitby 1975; Flagan 1999). Fundamentally, the width of the transfer function will govern the resolution with which two diameters can be separated. If the diameter bins are spaced such that the transfer functions do not overlap, then the flow ratio determines the diameter bin resolution. Better resolution may be achievable by working with overlapping bins but eventually will be limited by the selected flow ratios. For example, at a typical flow ratio of 10:1, the bin resolution for sizing 300 nm particles is ±22 nm. If the dry particle diameter is 100 nm, the uncertainty in the growth factor due to bin resolution alone is $2.8 < gf < 3.2$. This range severely limits the accuracy with which measured growth factors, together with the controlled RH, can be used in the calculation of water activity (Kreidenweis et al. 2005).

Some of these problems were highlighted by recent HTDMA intercomparisons (Duplissy et al. 2009; Good et al. 2010; Massling et al. 2011). These studies collectively show that HTDMA RH set points and the reported growth factors can be highly uncertain. For example, Massling et al. (2011) report that measurements of ammonium sulfate exhibit deviations equivalent to 4.5% RH from the set point of 90% RH. Problems associated with the HTDMA technique have spurred the community to find alternative methods of measuring aerosol hygroscopic growth. Two of these methods are the Leipzig Aerosol Cloud Interaction Simulator (LACIS; Wex et al. 2005) and the inverted streamwise-gradient cloud condensation nuclei counter (Ruehl et al. 2010). Both methods feature exceptional RH control but their scope is limited by the optical detectors used to determine the wet particle size distribution. The optical detectors measure particles of diameter >~300 nm and are subject to limitations in accuracy resolution, i.e., uncertainties in refractive index and in the conversion from optical to physical diameter.

Here we introduce a new HTDMA instrument designed to circumvent some of the above problems associated with RH control and growth factor resolution such that the precision in measured hygroscopicity and activity coefficients is improved to ±20%. We demonstrate this precision by presenting data for glucose and maleic acid for which the activity coefficients near water saturation are known with high accuracy.

2. INSTRUMENT DESIGN

2.1. Chemicals Used

The following chemicals were used: ammonium sulfate, 99.9% pure (Sigma-Aldrich); D-(+)- glucose, 99.5% pure (Fisher); maleic acid, reagent grade (Fisher).

2.2. Aerosol Generation

Figure 1 summarizes the setup of the HTDMA instrument. Aerosol is generated by atomizing an organic or ammonium sulfate solution and then drying the resulting aerosol. Two separate atomizers (TSI 3076) contain solutions of an organic compound or ammonium sulfate in deionized water (~18.2 MΩ cm) at 0.11 ± 0.03% mass concentration, mixed 0–4 days prior to use. Air from a zero-air generator (Teledyne 701) is directed to one of the two atomizers by a three-way solenoid valve, allowing automated control over the aerosol source. Aerosol from the active atomizer is routed through two silica diffusion dryers with liquid traps (TSI 3062) and a dilution setup. The dilution setup releases excess flow from the atomizers and removes a fraction of the aerosol by routing it though a HEPA filter and a flow restrictor in parallel. The aerosol then passes through a delay volume submerged in a temperature-controlled cold bath (Thermo Scientific, Pheonix II) kept at −20°C, which ensures that the dew point of the sample flow remained below 0°C (the aerosol has ~30 s transit time inside 0.635 cm inner diameter silicon tubing, during which it approaches ambient temperature). The dry aerosol stream is passed to through a ^{210}Po neutralizer to return it to an equilibrium charge distribution for size-selection by electric mobility.

2.3. DMA-I

After the second drying, the aerosol stream is at low RH (<15%) and passes into a high-flow differential mobility particle sizer (DMA-I) (Stolzenburg et al. 1998) at sheath:sample flow ratio of ~15:0.5 LPM. The DMA column has radial dimensions $r_1 = 5$ cm, $r_2 = 5.8$ cm, and length $L = 60$ cm. The sheath flow is circulated by a diaphragm pump (Gast, DOA-P707-AA) with two critical orifi (O'Keefe Controls Co.) and is filtered (Whatman glass microfiber HEPA-CAP™). DMA-I is neither insulated nor temperature controlled, and its temperature is slightly warmer than the room due to heat released by

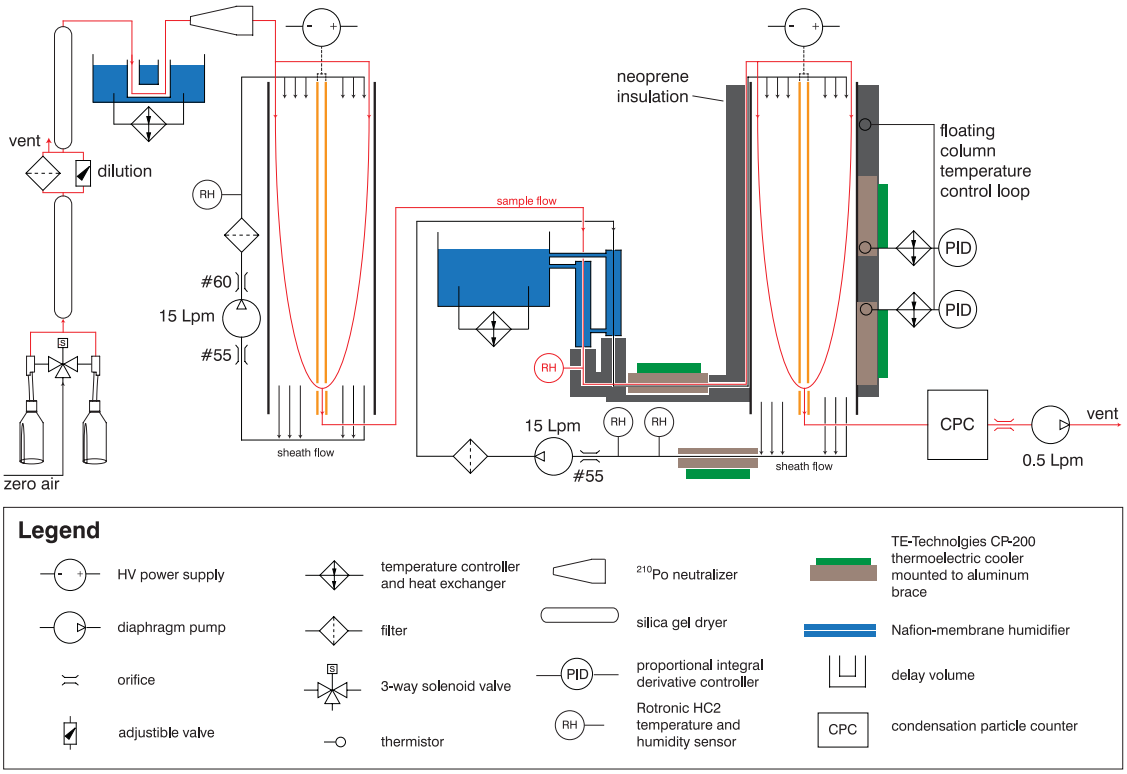

FIG. 1. Schematic of the instrument setup. (Color figure available online.)

the pumps and other electronic equipment located inside the instrument rack.

2.4. Humidification

The aerosol sample stream and the DMA-II sheath flow are each humidified by passage through a Nafion tube (PermaPure, MH-series, 0.279 cm outer diameter, 30.5 cm long) attached to a programmable temperature control bath (PolyScience, $\pm 0.01^{\circ}$C accuracy). The semipermeable Nafion membrane allows water at the specified temperature to evaporate into the air flow. The set temperature of the Nafion corresponds to the dew point needed to create the desired RH, given the temperature of DMA-II and with an empirically determined offset to account for imperfect efficiency of humidification. The residence time between the humidifier and DMA-II is $\sim$6 s, which is enough time to equilibrate to this new RH such that the measured size reflects the growth factor at the measured RH (Snider and Petters 2008), provided that there are no kinetic limitations to water uptake which may bias HTDMA results (Sjogren et al. 2007). The humidity in the Nafion flow area approaches 100% RH, as a function of the flow rate and Nafion age. Thus, the sample can deliquesce here and remain in a metastable state despite the RH falling later in the stream. Although the sheath flow is much faster than the sample flow, the difference in humidification efficiency is small ($\Delta T_{\mathrm{dew}} < \sim 0.5^{\circ}$C) because the sheath flow is recirculating through the Nafion and the sample flow enters dry. We expect the sheath and sample flows to reach the same RH and the particle wet diameter to adjust within a short distance after entering DMA-II (Snider et al. 2006; Snider and Petters 2008). Particle sizing uncertainties introduced by an RH mismatch (Biskos et al. 2006) would be most pronounced at high RH, and we have accounted for this by frequent calibration with ammonium sulfate.

2.5. DMA-II

The second DMA is of the same make and model as DMA-I, but is thermally insulated using several layers of 1″ neoprene and is actively temperature controlled. The DMA column is encased by aluminum sleeves that have thermoelectric heat exchangers (TE Technology CP-200) mounted on the outside. Two thermistors (Tetech MP-3193) are mounted to the aluminum sleeve near the heat exchanger. A third thermistor (TE Technology MP-3193) is mounted at the inlet of the DMA column. The thermistors have precision $\pm 0.01^{\circ}$C and are calibrated at 20°C against the temperature of the controlled water bath that is used to control the Nafion temperature. The thermistor temperature at the top of the DMA column is used as the set point for controlling the thermoelectric heat exchangers and thus for controlling the temperature at the middle and bottom of the column. Control is handled via external PID controllers (TE Technology TC-36–25-RS232) that receive a new set point every two seconds. The standard deviation of the three temperatures is less than $\pm 0.02^{\circ}$C inside an air-conditioned room, and absolute temperature varies $\sim 0.4^{\circ}$C over a 1–2 h time window.

Sheath and sample flow temperature and RH are preconditioned prior to entering DMA-II. Preconditioning is handled by routing the flows through a four-pass loop heat exchanger (TE Technologies LC-061) whose temperature is controlled independently from the column. The flows are then routed through the aluminum sleeve and in close contact with the column exterior, beneath the layer of insulation, to thermally equilibrate them with the DMA. A thermistor measures the temperature where the flows enter proximity with the column, and temperature of the preconditioning heat-exchanger is set such that the sheath flow entry temperature and that of the column-bottom aluminum heat exchanger mounting match as closely as possible. A second four-pass loop heat exchanger (TE Technologies LC-061) is mounted at the exit of DMA-II and its temperature is set 20°C warmer than that of DMA-II column. This warms the sheath flow to prevent condensation in the line.

All humidified lines are insulated with 1″ neoprene. Inline capacitive sensors (HC2 Rotronics, Hygroclip) measure the temperature and RH of the sample just prior to entry into DMA-II and the sheath flow after the exit of the second four-pass loop heat exchanger. Two RH sensors ensure redundancy of the measurement to better diagnose errors due to inadvertent flow saturation downstream of DMA-II. The sheath flow is circulated by a diaphragm pump (Gast, DOA-P707-AA) outfitted with a critical orifice (O'Keefe Controls Co., metal orifice #55) and an upstream filter. Particle concentration is counted by a condensation particle counter (CPC; TSI 3772) whose flow rate is reduced to 0.5 Lpm using a needle valve and verified using a bubble cell flow meter. The resulting sheath:sample flow ratio is ∼15:0.5.

3. EXPERIMENTAL METHODS AND DATA REDUCTION

3.1. Scanning Strategy

The humidified size distribution is measured for 100 nm dry particles. DMA-II and the CPC select and count particles starting at 80 nm and ending at 450 nm. Size scans were performed in differential mobility particle sizer (DMPS) mode. This mode was chosen over the scanning mobility particle sizer mode (SMPS) because the DMA transfer function is narrower for DMPS and requires a simpler data inversion technique, although in the future the instrument will feature SMPS mode scanning to increase data collection speed. Diameter bins were set such that the upper edge of the DMA-II transfer function of bin i coincided with the lower edge of the transfer function of bin $i + 1$. For each bin, concentration data were collected for ∼4 s after waiting one flush time for the DMA-II column to equilibrate to the newly set voltage. To speed up the measurement, the scan ranges are adjusted to measure the size distribution only near the expected growth factor. An expected range in hygroscopicity of the measured aerosol and the instantaneous RH measured are used to create a dynamic growth factor window, shortening the full scan duration of the humidified size distribution from about 15 min to about 8 min. The humidified size distribution was inverted using the TDMAfit algorithm (Stolzenburg and McMurry 1988; Zhou et al. 2002). This algorithm fits a Gaussian growth factor probability density function to match the observed mobility distribution that is expected from transfer through DMA-I and DMA-II. For each scan, the peak of the diameter probability density function obtained from the inversion is recorded as the measured D.

3.2. Derivation of Column RH

The DMA-II RH is derived from three column exterior temperatures and from the dew point temperature inferred from two RH sensors in line with the sheath flow via the Clausius–Clapeyron relationship. The column exterior temperatures are obtained from thermistors at the top, middle, and bottom of the column associated with the temperature controlling heat exchangers. The sheath flow is heated after passage through the column to prevent condensation and the dew point temperature is measured at RH much lower than column RH. The sensor-derived column RH associated with each growth factor is the average over that diameter duration, and is denoted as $RH(T,T_{dew})$.

3.3. Calibration of RH

At RH >90%, uncertainty in the column RH grows large due to accuracy limitations of the Rotronic RH sensors. We circumvent this problem by calibrating the instrument RH by alternating between organic scans and calibration scans with ammonium sulfate. The calibration scans are performed roughly every 20 min. The Extended Aerosol Inorganic Model (E-AIM) (Clegg et al. 1998; Wexler and Clegg 2002) is used to model the expected growth factor versus RH for a particular dry diameter, $gf(RH, D_d)$. This relationship is inverted to determine the RH from the observation and is denoted as $RH(gf, D_d)$. Ammonium sulfate has been used as a calibration standard before for CCN studies (Snider et al. 2006; Rose et al. 2008; Christensen and Petters 2012) and also to define RH for optical tweezer experiments (Hanford et al. 2008). The uncertainty in the ammonium sulfate osmotic coefficient data underlying the E-AIM model is ±0.01 (Clegg 2007) and is negligible relative to uncertainties from the resolution of the growth factor measurement.

Figure 2 shows the tradeoff between the uncertainty in the sensor-derived and calibrated RH, denoted as $\Delta RH(T,T_{dew})$ and $\Delta RH(gf, D_d)$, as a function of instrument RH. $RH(T,T_{\mathrm{dew}})$ is precise to ∼±1% in absolute units, as determined from the manufacturer specifications. The precision in $RH(gf,D_d)$ is determined by the E-AIM modeled slope of the ammonium sulfate growth factor with respect to RH and by the uncertainty in the measured ammonium sulfate growth factor estimated from the DMA transfer function. Specifically, $\Delta RH(gf,D_d)$ is derived from the uncertainty in growth factor, Δgf, combined with the slope of the aforementioned line. Figure 2 shows that $\Delta RH(gf,D_d)$ are larger at low RH than at high RH, which is due to the relative lack of sensitivity of gf on RH at low RH. Above RH ∼90%, $RH(gf,D_d)$ becomes rapidly more precise

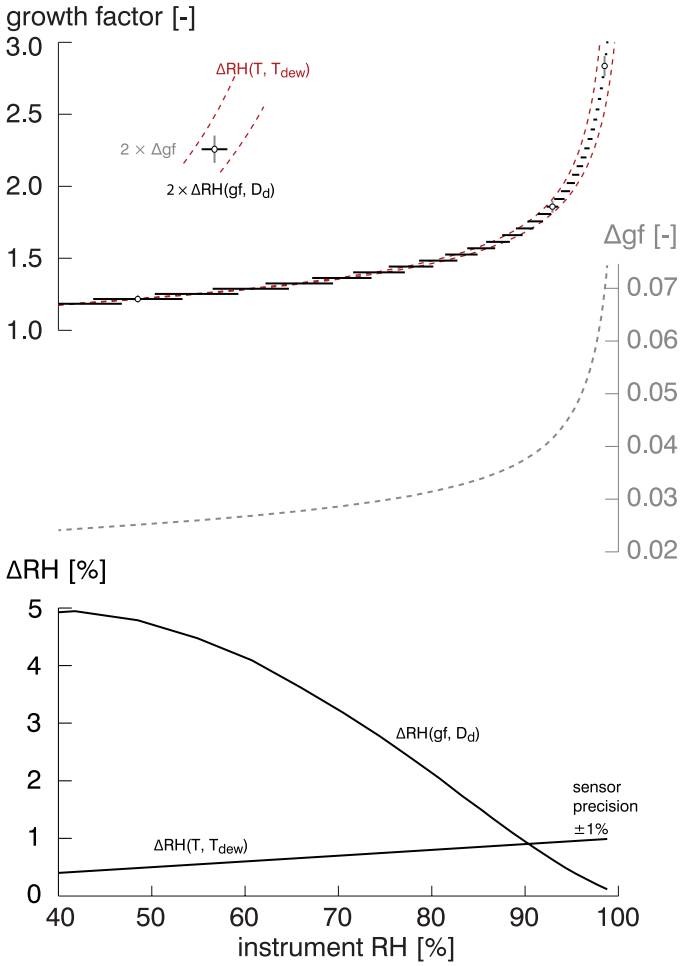

FIG. 2. Top panel: Ammonium sulfate growth factor as a function of RH, modeled by E-AIM. Vertical grey lines near the bottom left and the top right show $2 \times \Delta gf$, the uncertainty in growth factor from the DMA-II diameter resolution. Horizontal black lines show $2 \times \Delta RH(gf, D_d)$, the uncertainty in RH from the ammonium sulfate calibration. Dotted (red) lines show uncertainty in the RH sensor (±1%). Middle panel: Growth factor uncertainty as a function of RH, taking into account the DMA transfer function diameter dependence and ammonium sulfate hygroscopic growth RH dependence. Bottom panel: Uncertainty in $RH(gf, D_d)$ compared to uncertainty in $RH(T, T_{\text{dew}})$. (Color figure available online.)

than $RH(T,T_{\text{dew}})$. We therefore use $RH(gf,D_d)$ at RH $\geq$ 90% and $RH(T, T_{\text{dew}})$ at RH <90% to calibrate the humidity in our instrument.

Values of $RH(gf,D_d)$ are only defined at the time coinciding with the peak of the ammonium sulfate scan. We use the following procedure, illustrated in Figure 3, to obtain a calibrated RH value for each organic growth factor peak, denoted as RH_a. A calibration curve is constructed by fitting a line to the relationship between $RH(T,T_{\text{dew}})$ and $RH(gf,D_d)$ from the four nearest ammonium sulfate scans (Figure 3d). The fitted relationship is used with the instantaneous values of T and T_{dew} to compute RH_a.

3.4. System Stability

Figure 3 also illustrates the instrument temperature and RH stability. The three DMA-II column temperatures are nearly indistinguishable and the spread is $< \pm 0.02^{\circ}$C. The dew point temperature, controlled by the water bath temperature, is maintained at a constant offset relative to the column temperature. This results in a constant dew point depression and thus constant relative humidity. An overnight experiment at low RH resulted in $RH(T, T_{\text{dew}}) = 41 \pm 0.7\%$ (average ±standard deviation, 67 values ranging from 39.1 to 42.8%) and negligible change in maleic acid dry growth factors ($gf = 0.99 \pm 0.02$; average ± standard deviation, 32 values ranging from 0.9 to 1.07).

3.5. Shape Factor and DMA Agreement

Ammonium sulfate restructures upon humidification below its deliquescence RH (Biskos et al. 2006; Mikhailov et al. 2009). Irregularities in the dry particles can cause a discrepancy between the mobility equivalent and volume equivalent particle diameters. Because growth factors are referenced against the dry volume equivalent diameter, particle irregularities may bias the growth factor data. For example, a highly nonspherical particle with dry mobility equivalent diameter of 100 nm would have a much smaller volume equivalent diameter (e.g., 80 nm). If this particle were to grow hygroscopically by a factor 1.25, it would be measured as 100 nm wet particle and the detected gf would be 1. To account for restructuring, a factor is introduced that increases measured growth factors by a multiplicative scaling factor f (Kreidenweis et al. 2005):

$$gf = f\frac{D}{D_{d,me}}$$
$$f = \frac{\chi C_c(D_{d,me})}{C_c(D_{VE})}, \qquad [2]$$

where C_c is the Cunningham slip correction, χ is the dynamic shape factor, D_{VE} is the volume equivalent diameter and $D_{d,me}$ is the dry mobility equivalent diameter. This factor subsumes any sizing offset between DMAs (Gysel et al. 2009), a dynamic shape factor that converts between mobility and volume equivalent diameter (Kasper 1982), and void spaces that may be present in the particle (Weis and Ewing 1999; Ciobanu et al. 2010). The factor f can be found empirically by finding the value for which the measured gf of ammonium sulfate agrees best with E-AIM at RH <80%, where the error in RH is small relative to errors in particle sizing. For our setup, $f = 0.99$. This value was consistent between experiments, indicating slightly irregular particles, slightly offset DMAs, or both. Previous studies have reported χ ranging between 1.02 and 1.07 for ammonium sulfate particles ranging between 6 and 500 nm (Biskos et al. 2006; Zelenyuk et al. 2006). For a system with no DMA offset and assuming particles have no void spaces, these χ values correspond to an equivalent f ranging between 1.01 and 1.035 (Carrico et al. 2008). The sizing offset between two DMAs depends on flow calibration and stability, voltage calibration,

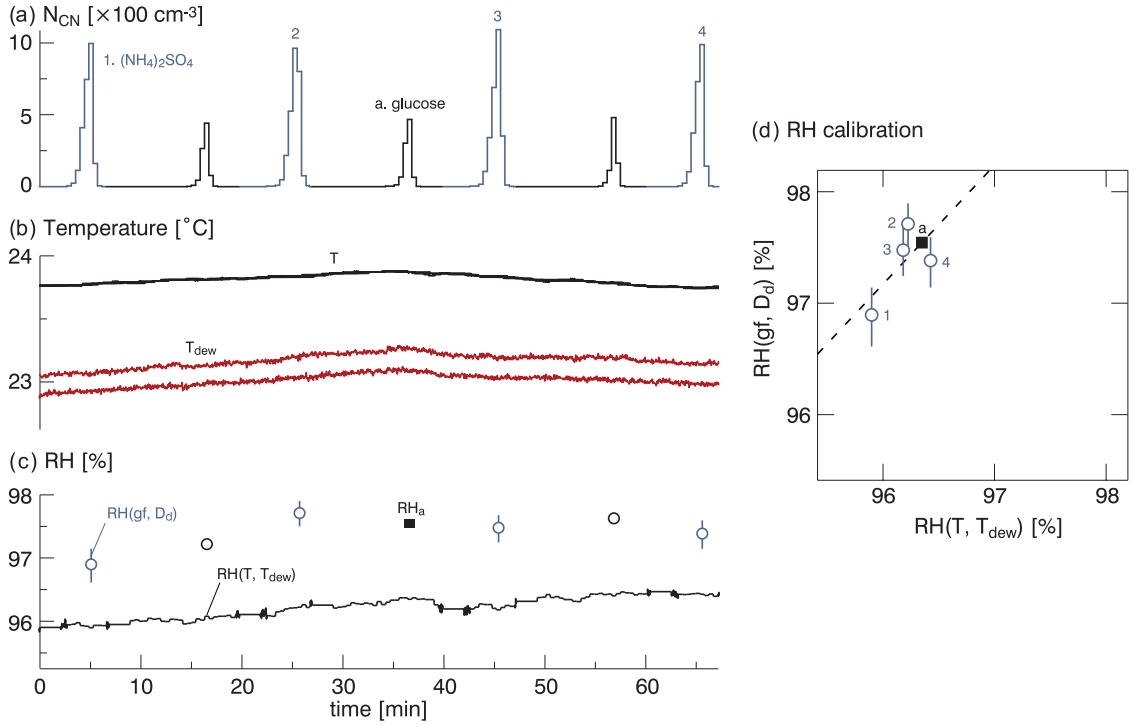

FIG. 3. (a) Timeseries of humidified growth factor peaks averaged over diameter bins for ammonium sulfate (grey [blue online]) and glucose (black). (b) Timeseries of three exterior DMA-II column temperatures (black) and two inline sheath flow dew point temperatures (grey [red online]). (c) Timeseries of $RH(T, T_{\mathrm{dew}})$ (black), $RH(gf, D_d)$ (gray circles [blue online]), RH_a (black circles). The black square corresponds to peak "a" in (a) and is calibrated by ammonium sulfate scans 1 through 4. (d) Comparison of $RH(T, T_{\mathrm{dew}})$ and $RH(gf, D_d)$. Numbers correspond to the numbered peaks in (a). Each RH_a is calibrated by a best-fit line through four closest ammonium sulfate scans (black square). (Color figure available online.)

and precision of DMA machining. We checked the sizing and agreement between DMA-I and DMA-II using polystyrene nanospheres (102 ± 3 nm, Thermo Scientific lot #36489) and the DMAs agreed within the uncertainty of this standard. We therefore conclude that our scaling factor of 0.99 is consistent with expected instrument precision and previously reported dynamic shape factors.

3.6. Thermodynamic Variables

The growth factor and RH data are further reduced to obtain the hygroscopicity parameter, osmotic coefficient, and activity coefficient as outlined in Petters et al. (2009) and references therein. The measured growth factor, gf_{meas}, is calculated from Equation (1). The activity of water, a_w, is calculated using D_d, gf_{meas}, and the adjusted RH_a (or $RH(gf,D_d)$ for ammonium sulfate) following Köhler theory (Kreidenweis et al. 2005):

$$a_w = \frac{RH_a}{100}\left(\exp\left(\frac{A}{gf_{\mathrm{meas}} D_d}\right)\right)^{-1}, \qquad [3]$$

where $A = \frac{4\sigma_{s/a} M_w}{\rho_w RT}$, $\sigma_{s/a}$ is the surface tension of the solution-air interface, M_w is the molar mass of water, ρ_w is the density of water, and R is the universal gas constant. We calculated A at a reference state of $T = 298.15$ K and $\sigma_{s/a} = 0.072$ J m^{-2}, i.e., that of pure water at 298.15 K (Christensen and Petters 2012). The hygroscopicity parameter, κ, was calculated from a_w and gf_{meas} (Petters and Kreidenweis 2007):

$$\kappa = \frac{\left(gf_{\mathrm{meas}}^3 - 1\right)(1 - a_w)}{a_w}. \qquad [4]$$

The ideal κ, κ_{ideal}, was calculated using known constants:

$$\kappa_{\mathrm{ideal}} = \nu_s \frac{M_w \rho_s}{M_s \rho_w}, \qquad [5]$$

where ν_s is the number of dissociable ions per dry solute unit, ρ_s is the solute density, and M_s is the solute molar mass. The osmotic coefficient, Φ, was calculated using κ and κ_{ideal} (Kreidenweis et al. 2005):

$$\phi = \frac{\kappa}{\kappa_{\mathrm{ideal}}}. \qquad [6]$$

The activity coefficient, γ, was calculated from gf_{meas}, κ_{ideal}, and a_w (Petters et al. 2009):

$$\gamma = a_w \frac{gf_{\mathrm{meas}}^3 - 1 + \kappa_{\mathrm{ideal}}}{gf_{\mathrm{meas}} - 1}. \qquad [7]$$

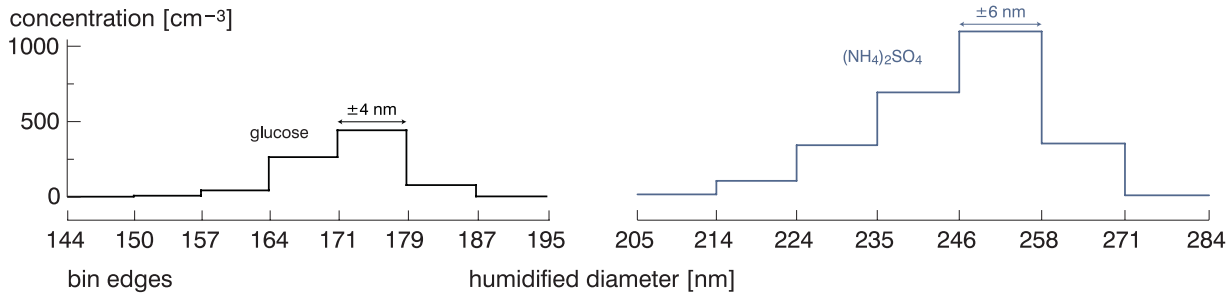

FIG. 4. Example histograms of particle number concentration versus size for glucose (left) and ammonium sulfate (right), with the diameter bin edges from the DMA-II transfer function denoted below. The dry diameter for these growth factors was 100 nm. Concentrations at diameters beyond the bins shown were zero. (Color figure available online.)

The mole fraction of water is related to the activity coefficient and the activity of water by

$$x_w = \frac{a_w}{\gamma}. \quad [8]$$

3.7. Precision

Figure 4 shows the histograms of particle number concentration versus size for glucose and for ammonium sulfate. The bin width is determined by the sheath:sample flow ratio and the theoretical transfer function from theory. Because the diameter bins were spaced such that they do not overlap, growth factor distributions should spread across two bins. This is expected because the DMA-II bin resolution is similar to that of DMA-I—although the dry distribution shifts by some factor gf, it should straddle at most two DMA-II diameter bins. Our data show some broadening beyond this expectation (which also occurred for dry scans), suggesting that the ideal transfer function is a lower estimate for our setup. Deviations from the ideal transfer function can occur due to maldistribution of aerosol in the inlet, turbulence, imperfections in the electrode geometry, and factors that may distort the flow or electric fields (Flagan 1999). We believe that we operate our DMA at the upper limit of sheath:sample flow ratio, thus explaining the deviation from ideal DMA theory.

The growth factor peak cannot be resolved more precisely than the diameter bin width, and this precision limit propagates to uncertainty in RH_a at RH > 90%. Further, uncertainty in RH_a and in the measured organic growth factor limits the precision of the thermodynamic variables that can be determined with the setup presented here. Figure 5 contours the maximum percent error in Φ as a function of RH_a and the organic κ value. The percent error was derived from the maximum deviation in κ derived from the extremes in gf and RH from the width of the transfer function at the organic diameter and at the diameter of the calibration ammonium sulfate aerosol. From this analysis we expect that better than ±20% precision for organic compounds of $\kappa > \sim 0.03$ for RH >90% is theoretically achievable.

4. RESULTS

4.1. Glucose

Figure 6 shows hygroscopic growth factors measured for glucose up to an RH of 98.9% along with the κ, Φ, and γ values for this data. The ammonium sulfate calibration data are included as solid symbols, with a line indicating the values modeled by E-AIM. At RH > 90%, the ammonium sulfate data are forced to the E-AIM line as part of the calibration. The agreement between measured and modeled ammonium sulfate at RH <90% shows that the data are not biased.

4.2. Margules Model

The Margules equation (Equation (9); Prausnitz et al. 1999; Petters et al. 2009) was fit to γ and x_w using a

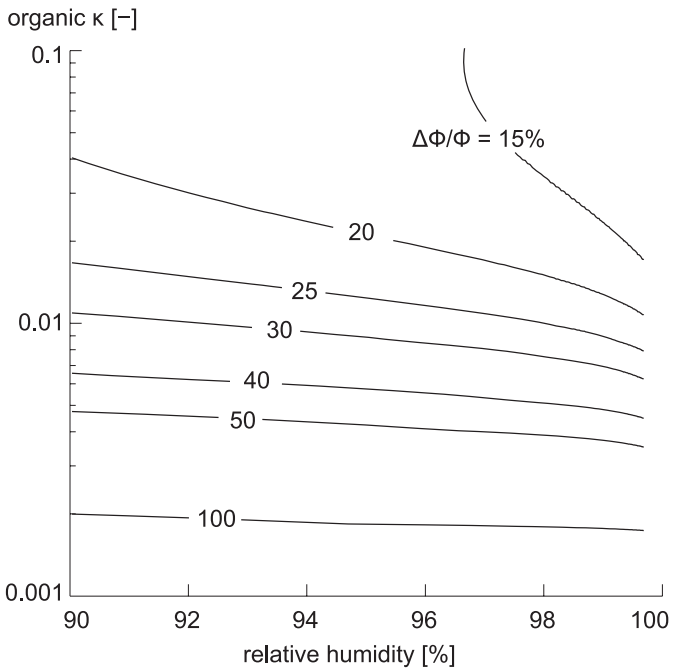

FIG. 5. Contours of uncertainty in Φ obtained using the uncertainty in calibrated RH and the uncertainty in measured organic growth factor. Uncertainty is taken to be half the range between maximum and minimum Φ, expressed as percent and denoted on the contour lines.

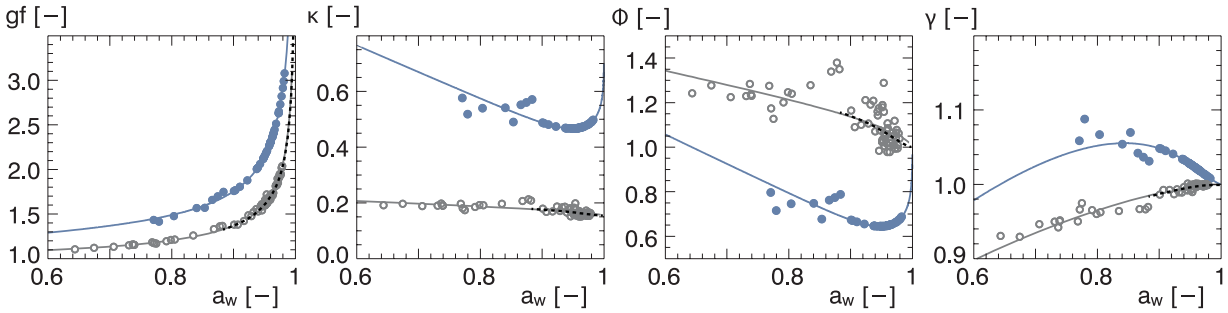

FIG. 6. Hygroscopic growth factor data for glucose (dark open circles), ammonium sulfate calibration (light solid circles), and glucose from Miyajima et al. (1983) (black dashed line). The dark solid line shows the Margules equation fit to the data (Equation (9); $\alpha = -0.3264$, $\beta = 1.2676$), and the light solid line shows the E-AIM model. The ammonium sulfate data are forced to the E-AIM line below 90% RH. The first panel shows hygroscopic growth factor (Equation (1)), the second shows the hygroscopicity parameter κ (Equation (4)), the third shows the osmotic coefficient ϕ (Equation (6)), and the fourth shows the activity coefficient γ (Equation (7)). (Color figure available online.)

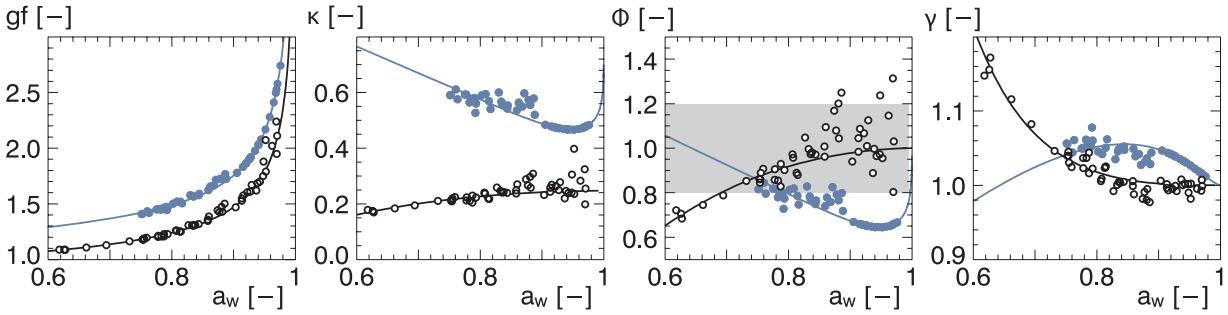

FIG. 7. Hygroscopic growth factor data for maleic acid (black open circles), similar to Figure 6. The shaded area shows the extent of the data from Clegg and Seinfeld (2006). (Color figure available online.)

trust-region-reflective algorithm (Coleman and Li 1996) to determine the parameters α_i and β_i:

$$\ln\gamma = \sum_{i=1} \alpha_i \, (1 - x_w)^{\beta_i} \, . \qquad [9]$$

The Margules parameters were derived because they can be directly ingested by models such as E-AIM (Clegg et al. 1992; Clegg et al. 2003). The Margules fit parameters for glucose were $\alpha = -0.3264$, $\beta = 1.2676$. This model is included in Figure 6 in all panels as a dark solid line. Comparison to bulk measurements by Miyajima et al. (1983) obtained with the isopiestic method (Figure 6, black dotted line), together with the observation that our data approach $\Phi = 1$ at high RH indicates that the data are unbiased. The $\pm 20\%$ scatter at high RH is consistent with the expected instrument precision (Figure 5).

4.3. Maleic Acid

Figure 7 shows hygroscopic growth factors for maleic acid up to an RH of 98.0%. The grey shaded area indicates the range reported for the same compound by Clegg and Seinfeld (2006). We point out that $\Phi > 1$ is expected for maleic acid at infinite dilution due to dissociation of the acid (e.g., Figure 6 in Clegg and Seinfeld 2006). This effect, however, is smaller than the $\pm 20\%$ precision achievable with our method and thus is unresolved here. The Margules model is plotted in all panels as a black line, and the Margules fit parameters were $\alpha = 1.2883$, $\beta = 2.7818$.

5. DISCUSSION AND CONCLUSIONS

We have demonstrated an HTDMA technique capable of measuring hygroscopic growth factors of metastable solutions. This technique results in unbiased water activity coefficients, precise within $\pm 20\%$. Our choice of compounds was limited to nearly spherical particles that are nonvolatile, do not alter surface tension, and do not exhibit kinetic limitations to hygroscopic growth. These assumptions may not always hold. For example, Mikhailov et al. (2009) found that oxalic acid, although it has a low vapor pressure, may evaporate during processing. The passage between humidification and size distribution measurement is short, making kinetic limitations to water uptake a concern. However, shorter residence times also minimize potential biases due to volatility between the DMAs. The presence of surfactants may bias the inferred water activity via Equation (3). In this case, a more sophisticated theory that accounts for the radial surfactant partitioning within the droplet (Sorjamaa et al. 2004; Li et al. 1998; Petters and Kreidenweis 2012) may be needed to accurately infer water activity from growth factor data. We also assumed that the same scaling factor (i.e., dynamic shape factor) applies to the organic compounds and the

ammonium sulfate. An offset in the two scaling factors could bias our data, although this offset may be noticeable if Φ does not approach 1 at infinite dilution. The calculation of Φ and γ relies on known molar mass, density, and number of dissociable ions. Without this knowledge of particle composition, ideal behavior is unknown and only growth factor and κ can be determined.

The presented HTDMA method has the advantage over optical methods (Wex et al. 2005; Ruehl et al. 2010) of being able to examine the growth factor of particles in the 30 to 200 nm size range. Unlike optical methods, the HTDMA method does not require input of the refractive index and can measure growth factors for strongly absorbing aerosol such as black carbon.

This instrument is subject to limitations in particle size and scan time stemming from the geometry of the DMA columns and from the tradeoff between instrument precision and speed. The upper limit of voltage applied to DMA-II is 10 kV and sets the highest humidified particle diameter near 1 μm. The upper dry diameter limit depends on the hygroscopicity of the reference material for RH calibration and the highest desired RH. For the ammonium sulfate system, $gf = 4$ corresponds to RH = 99.7%. Therefore, 200 nm dry particles can be used to characterize an aerosol that is less hygroscopic than ammonium sulfate. The instrument features conflicting design criteria for temporal versus RH resolution. Precision is determined by the spacing of the diameter bins and thus the sheath:sample flow ratio. In principle, the minimum sampling time per bin is determined until a threshold count is received by the CPC. For a faster DMPS scan, some size resolution must be sacrificed.

REFERENCES

Amundson, N. R., Caboussat, A., He, J. W., Martynenko, A. V., Landry, C., Tong, C. et al. (2007). A New Atmospheric Aerosol Phase Equilibrium Model (UHAERO): Organic Systems. *Atmos. Chem. Phys.*, 7(17):4675–4698.

Barrett, E. W., and Herndon, L. R. (1951). An Improved Electronic Dew-Point Hygrometer. *J. Meteor.*, 8(1):41–51.

Biskos, G., Paulsen, D., Russell, L. M., Buseck, P. R., and Martin, S. T. (2006). Prompt Deliquescence and Efflorescence of Aerosol Nanoparticles. *Atmos. Chem. Phys.*, 6(12):4633–4642.

Carrico, C. M., Petters, M. D., Kreidenweis, S. M., Collett, J. L., Jr., Engling, G., and Malm, W. C. (2008). Aerosol Hygroscopicity and Cloud Droplet Activation of Extracts of Filters From Biomass Burning Experiments. *J. Geophys. Res.*, 113:D08206.

Christensen, S. I., and Petters, M. D. (2012). The Role of Temperature in Cloud Droplet Activation. *J. Phys. Chem. A*, 116(39):9706–9717.

Ciobanu, V. G., Marcolli, C., Krieger, U. K., Zuend, A., and Peter, T. (2010). Efflorescence of Ammonium Sulfate and Coated Ammonium Sulfate Particles: Evidence for Surface Nucleation. *J. Phys. Chem. A*, 114(35):9486–9495.

Clegg, S. L. (2007). Interactive Comment on "Calibration and Measurement Uncertainties of a Continuous-Flow Cloud Condensation Nuclei Counter (DMT-CCNC): CCN Activation of Ammonium Sulfate and Sodium Chloride Aerosol Particles in Theory and Experiment" by D. Rose et al. *Atmos. Chem. Phys. Discuss.*, 7(3):S4180–S4183.

Clegg, S. L., Brimblecombe, P., and Wexler, A. S. (1998). Thermodynamic Model of the System H^+– NH_4^+– Na^+– SO_4^{2-}– NO_3^-– Cl^-– H_2O at 298.15 K. *J. Phys. Chem. A*, 102(12):2155–2171.

Clegg, S. L., Pitzer, K. S., and Brimblecombe, P. (1992). Thermodynamics of Multicomponent, Miscible, Ionic Solutions. Mixtures Including Unsymmetrical Electrolytes. *J. Phys. Chem.*, 96(23):9470–9479.

Clegg, S. L., and Seinfeld, J. H. (2006). Thermodynamic Models of Aqueous Solutions Containing Inorganic Electrolytes and Dicarboxylic Acids at 298.15 K. 1. The Acids as Nondissociating Components. *J. Phys. Chem. A*, 110(17):5692–5717.

Clegg, S. L., Seinfeld, J. H., and Edney, E. O. (2003). Thermodynamic Modelling of Aqueous Aerosols Containing Electrolytes and Dissolved Organic Compounds. II. An Extended Zdanovskii–Stokes–Robinson Approach. *J. Aerosol Sci.*, 34(6):667–690.

Coleman, T. F., and Li, Y. (1996). An Interior Trust Region Approach for Nonlinear Minimization Subject to Bounds. *SIAM J. Optim.*, 6(2):418–445.

Duplissy, J., Gysel, M., Sjogren, S., Meyer, N., Good, N., Kammermann, L., et al. (2009). Intercomparison Study of Six HTDMAs: Results and Recommendations. *Atmos. Meas. Tech.*, 2(2):363–378.

Flagan, R. C. (1999). On Differential Mobility Analyzer Resolution. *Aerosol Sci. Tech.*, 30(6):556–570.

Good, N., Topping, D. O., Duplissy, J., Gysel, M., Meyer, N. K., Metzger, A., et al. (2010). Widening the Gap Between Measurement and Modelling of Secondary Organic Aerosol Properties? *Atmos. Chem. Phys.*, 10(6):2577–2593.

Gysel, M., McFiggans, G. B., and Coe, H. (2009). Inversion of Tandem Differential Mobility Analyser (TDMA) Measurements. *J. Aerosol Sci.*, 40(2):134–151.

Hanford, K. L., Mitchem, L., Reid, J. P., Clegg, S. L., Topping, D. O., and McFiggans, G. B. (2008). Comparative Thermodynamic Studies of Aqueous Glutaric Acid, Ammonium Sulfate and Sodium Chloride Aerosol at High Humidity. *J. Phys. Chem. A*, 112(39):9413–9422.

Hennig, T., Massling, A., Brechtel, F. J., and Wiedensohler, A. (2005). A Tandem DMA for Highly Temperature-Stabilized Hygroscopic Particle Growth Measurements Between 90% and 98% Relative Humidity. *J. Aerosol Sci.*, 36(10):1210–1223.

Kasper, G. (1982), Dynamics and Measurement of Smokes. Size Characterization of Nonspherical Particles. *Aerosol Sci. Tech.*, 1(2), 187–199.

Knutson, E. O., and Whitby, K. T. (1975). Aerosol Classification by Electric Mobility: Apparatus, Theory, and Applications. *J. Aerosol Sci.*, 6(6):443–451.

Kreidenweis, S. M., Koehler, K., DeMott, P. J., Prenni, A. J., Carrico, C., and Ervens, B. (2005). Water Activity and Activation Diameters from Hygroscopicity Data – Part I: Theory and Application to Inorganic Salts. *Atmos. Chem. Phys.* 5(5):1357–1370.

Li, Z., Williams, A. L., and Rood, M. J. (1998). Influence of Soluble Surfactant Properties on the Activation of Aerosol Particles Containing Inorganic Solute. *J. Atmos. Sci.*, 55(10):1859–1866.

Massling, A., Niedermeier, N., Hennig, T., Fors, E. O., Swietlicki, E., Ehn, M., et al. (2011). Results and Recommendations from an Intercomparison of Six Hygroscopicity-TDMA Systems. *Atmos. Meas. Tech.*, 4(3):485–497.

Mikhailov, E., Vlasenko, S., Martin, S. T., Koop, T., and Pöschl, U. (2009). Amorphous and Crystalline Aerosol Particles Interacting with Water Vapor: Conceptual Framework and Experimental Evidence for Restructuring, Phase Transitions and Kinetic Limitations. *Atmos. Chem. Phys.*, 9(24):9491–9522.

Miyajima, K., Sawada, M., and Nakagaki, M. (1983). Studies on Aqueous Solutions of Saccharides. I. Activity Coefficients of Monosaccharides in Aqueous Solutions at 25°C. *Bull. Chem. Soc. Jpn.*, 56(6):1620–1623.

Petters, M. D., and Kreidenweis, S. M. (2007). A Single Parameter Representation of Hygroscopic Growth and Cloud Condensation Nucleus Activity. *Atmos. Chem. Phys.*, 7(8):1961–1971.

Petters, M. D., and Kreidenweis, S. M. (2013). A Single Parameter Representation of Hygroscopic Growth and Cloud Condensation Nucleus Activity – Part 3: Including Surfactant Partitioning. *Atmos. Chem. Phys.*, 13, 1081–1091.

Petters, M. D., Wex, H., Carrico, C. M., Hallbauer, E., Massling, A., McMeeking, G. R., et al. (2009). Towards Closing the Gap Between

Hygroscopic Growth and Activation for Secondary Organic Aerosol – Part 2: Theoretical Approaches. *Atmos. Chem. Phys.*, 9(12):3999–4009.

Prausnitz, J. M., Lichtenthaler, R. N., and de Azevedo, E. G. (1999). *Molecular Thermodynamics of Fluid-Phase Equilibria.* Prentice Hall, Upper Saddle River, New Jersey, USA, p. 226.

Prenni, A. J., Petters, M. D., Kreidenweis, S. M., DeMott, P. J., and Ziemann, P. J. (2007). Cloud Droplet Activation of Secondary Organic Aerosol. *J. Geophys. Res.*, 112:D10223.

Raatikainen, T., and Laaksonen, A. (2005). Application of Several Activity Coefficient Models to Water-Organic-Electrolyte Aerosols of Atmospheric Interest. *Atmos. Chem. Phys.*, 5(9):2475–2495.

Rader, D. J., and McMurry, P. H. (1986). Application of the Tandem Differential Mobility Analyzer to Studies of Droplet Growth or Evaporation. *J. Aerosol Sci.*, 17(5):771–787.

Rose, D., Gunthe, S. S., Mikhailov, E., Frank, G. P., Dusek, U., Andreae, M. O., et al. (2008). Calibration and Measurement Uncertainties of a Continuous-Flow Cloud Condensation Nuclei Counter (DMT-CCNC): CCN Activation of Ammonium Sulfate and Sodium Chloride Aerosol Particles in Theory and Experiment. *Atmos. Chem. Phys.*, 8(5):1153–1179.

Ruehl, C. R., Chuang, P. Y., and Nenes, A. (2010). Aerosol Hygroscopicity at High (99 to 100%) Relative Humidities. *Atmos. Chem. Phys.*, 10(3):1329–1344.

Sjogren, S., Gysel, M., Weingartner, E., Baltensperger, U., Cubison, M. J., Coe, H., et al. (2007). Hygroscopic Growth and Water Uptake Kinetics of Two-Phase Aerosol Particles Consisting of Ammonium Sulfate, Adipic and Humic Acid Mixtures. *J. Aerosol Sci.*, 38(2):157–171.

Snider, J. R., and Petters, M. D. (2008). Optical Particle Counter Measurement of Marine Aerosol Hygroscopic Growth. *Atmos. Chem. Phys.*, 8(7):1949–1962.

Snider, J. R., Petters, M. D., Wechsler, P., and Liu, P. S. K. (2006). Supersaturation in the Wyoming CCN Instrument. *J. Atmos. Oceanic Technol.*, 23(10):1323–1339.

Sorjamaa, R., Svenningsson, B., Raatikainen, T., Henning, S., Bilde, M., and Laaksonen, A. (2004). The Role of Surfactants in Köhler Theory Reconsidered. *Atmos. Chem. Phys.*, 4(8):2107–2117.

Stolzenburg, M., Kreisberg, N., and Hering, S. (1998). Atmospheric Size Distributions Measured by Differential Mobility Optical Particle Size Spectrometry. *Aerosol Sci. Tech.*, 29(5):402–418.

Stolzenburg, M. R., and McMurry, P. H. (1988). TDMAfit User's Manual. *Particle Technology Laboratory Publications* 653, Dept. of Mech. Engr., U. Minnesota, Minneapolis, MN.

Topping, D. O., McFiggans, G. B., and Coe, H. (2005). A Curved Multi-Component Aerosol Hygroscopicity Model Framework: Part 2 – Including Organic Compounds. *Atmos. Chem. Phys.*, 5(5):1223–1242.

Weingartner, E., Gysel, M., and Baltensperger, U. (2002). Hygroscopicity of Aerosol Particles at Low Temperatures. 1. New Low-Temperature H-TDMA Instrument: Setup and First Applications. *Environ. Sci. Technol.*, 36(1):55–62.

Weis, D. D., and Ewing, G. E. (1999). Water Content and Morphology of Sodium Chloride Aerosol Particles. *J. Geophys. Res.*, 104:21275–21285.

Wex, H., Kiselev, A., Stratmann, F., Zoboki, J., and Brechtel, F. J. (2005). Measured and Modeled Equilibrium Sizes of NaCl and $(NH_4)_2SO_4$ Particles at Relative Humidities up to 99.1%. *J. Geophys. Res.*, 110:D21212.

Wexler, A. S., and Clegg, S. L. (2002). Atmospheric Aerosol Models for Systems Including the Ions H^+, NH_4^+, Na^+, SO_4^{2-}, NO_3^-, Cl^-, Br^-, and H_2O. *J. Geophys. Res.*, 107(D14):4207.

Zelenyuk, A., Cai, Y., and Imre, D. (2006). From Agglomerates of Spheres to Irregularly Shaped Particles: Determination of Dynamic Shape Factors from Measurements of Mobility and Vacuum Aerodynamic Diameters. *Aerosol Sci. Tech.*, 40(3):197–217.

Zhou, J., Swietlicki, E., Hansson, H. C., and Artaxo, P. (2002). Submicrometer Aerosol Particle Size Distribution and Hygroscopic Growth Measured in the Amazon Rain Forest During the Wet Season. *J. Geophys. Res.*, 107:8055.